Available online at www.sciencedirect.com
SCIENCE DIRECT®
Nuclear Instruments and Methods in Physics Research A 497 (2003) 141–149
NUCLEAR INSTRUMENTS & METHODS IN PHYSICS RESEARCH Section A
www.elsevier.com/locate/nima

Imaging of breast phantoms using a high-resolution position sensitive photomultiplier tube

N.D. Giokaris[a,c,*], G.K. Loudos[b], D. Maintas[e], D. Papapanagiotou[e], K.S. Nikita[b], N.K. Uzunoglu[b], A. Karabarbounis[a], C.N. Papanicolas[a,c], E. Stiliaris[a], S.C. Archimandritis[d], A.D. Varvarigou[d], C.N. Stefanis[f], S. Majewski[g], A. Weisen-berger[g], R. Pani[h], F. Scopinaro[h]

[a] *Institute of Accelerating Systems and Applications, P.O. Box 17214, 10024 Athens, Greece*
[b] *National Technical University of Athens, Iroon Polytexneiou 9, Zografos, 15773 Athens, Greece*
[c] *National Capodistrian University of Athens, Panepistimiou 30, 10679 Athens, Greece*
[d] *National Center for Scientific Research "Demokritos", Aghia Paraskevi, 15310 Athens, Greece*
[e] *Athens Medical Center Institute of Isotopic Studies, Distomou 5-7, Marousi, 15125 Athens, Greece*
[f] *University Mental Health Research Institute, Dimitressa 10, 115 21 Athens, Greece*
[g] *"Jefferson Lab", Newport News, Virginia, USA*
[h] *University of Rome "La Sapienza", Rome, Italy*

Abstract

The results of studies conducted with a small field of view gamma camera based on a Position Sensitive Photomultiplier Tube (PSPMT) and a pixelized scintillator crystal, made of CsI(Tl), are reported. Using a computer-controlled step motor allowing object rotation, projection data from several angles are acquired. Images of slices of the object are obtained and compared with the use of a Filtered Backprojection and a Maximum Likelihood algorithm. Phantom studies have shown a spatial resolution of 2–3 mm in both two and three dimensions, and mice experiments have shown successful SPECT imaging of small organs. 3D images obtained from a paraffin cylinder phantom and from a ^{99m}Tc water solution phantom showed that a "hot" spot with a size down to 0.2 ml can be detected with a resolution of about 2 mm if the tumor to background activity ratio is 6:1.

Keywords: PSPMT; Breast phantoms; High resolution; Sensitivity; Maximum likelihood; "Hot" spot

1. Introduction

The basic detector element of clinical SPECT systems is based on Anger camera [1], which offers a spatial resolution of 4–6 mm. A typical camera consists of an array of photomultiplier tubes that have their entrance windows coupled by light guides to a large plate of a crystal scintillator material. The location of the interaction point is determined from the relative intensity of the light pulse signal simultaneously detected by all of the

*Corresponding author. Tel.: +30-1-725-733.
E-mail address: ngiokar@cc.uoa.gr (N.D. Giokaris).

0168-9002/03/$ - see front matter
PII: S0168-9002(02)01904-6

photomultiplier tubes. High-resolution images are obtained by choosing high-resolution collimators and photon detectors with high intrinsic position resolving capability.

Dedicated gamma cameras for specific clinical applications, which are based on PSPMTs, are representing a new trend in nuclear medicine [2]. Two-dimensional (2D) studies have shown that, by coupling a YAP, Cs(Tl) or NaI(Tl) scintillation crystal to a PSPMT, a spatial resolution as high as 2 mm can be achieved [3, 4].

The commercial availability of larger field of view PSPMTs and the continuing development of higher detection efficiency scintillation crystals and light guides permit the development of relatively low-cost high-resolution scintimammography detectors. Thus, information on functional or metabolic tumor activity that is complementary to the structural information of X-ray mammography can be provided potentially reducing the number of unnecessary biopsies and missed cancers [5].

Tomography and 3D imaging have been a research field where contribution of many scientific areas has resulted to a great number of methods and tools for 3D reconstruction and visualization of an object when a number of projections is known. Convention SPECT systems, which have been used for the past three decades, suffer from low resolution and limited number of the detected counts, due to their basic detector elements, since they are still based on Anger camera [6].

The aim of the present work was to examine if a small field of view high-resolution device developed for small animal imaging can successfully produce tomographic images of small breast tumors. Our SPECT system is based on a PSPMT, a CAMAC plus associated electronics and a computer controlled step motor [7]. Phantom tests as well as experiments in normal mice using conventional radiopharmaceuticals, and in tumor-bearing nude mice using radiopharmaceuticals under development, have been carried out both in two and three dimensions [8]. In this preliminary study, slices were obtained using a Filtered Backprojection (FBP) [9,10] and a Maximum Likelihood (MLA) [11,12] algorithm.

2. Experimental setup and data acquisition

The gamma camera consists of a R2486 Hamamatsu PSPMT equipped with 8×8 crossed-wire anode wire pairs. A 2.7 cm thick collimator with 1.22 mm diameter hexagonal holes and a 4.5 cm in diameter CsI(Tl) crystal pixelized in 1.13 mm^2 cells are used in conjunction with the PSPMT, for photon detection.

The signals of the anodes are preamplified through 16 preamplifiers (LeCroy TRA1000) and then transferred to a CAMAC system, which hosts an ADC (LeCroy FERA 4300B), a memory (LeCroy FERA 4302), a driver (LeCroy FERA 4301) and a controller (Jorway 73A). The digital signals are transported to a G3 Power Mac via a SCSI bus. The signal from the last dynode is inverted, amplified, passed through a discriminator (LeCroy 821) and used for ADC gating. Specific software (Kmax 6.4.5-Sparrow Corporation) allows CAMAC programming, system calibration, data acquisition and signal processing.

A computer-controlled step motor (MD-2 ARRICK Robotics) allows object rotation around an axis perpendicular to the camera axis. Thus, projection data from several angles can be acquired. Fig. 1 shows the experimental configuration.

The readout of the signals from a PSPMT has been presented extensively elsewhere [4]. An incident photon interacts with the CsI detector and produces scintillation light. The scintillation strikes the photocathode and liberates photoelectrons, which are multiplied at a 12 dynode system by an electric potential of typically 950 V for ^{99m}Tc. Thus, an electron cloud reaches the crossed wire anode stage. Readout of the 16 anode signals allows calculation of the centre of gravity (COG) of the electron cloud and consequently determination of the exact position of the incident photon in the XY plane. To avoid edge effects [4] anode wires that carry small signals (less than 5–10% of the total anode signal) are disregarded in the COG calculation.

Calibration of the system is carried out using a flood source in order to correct non-uniformity in spatial efficiency of the crystal and the collimator. Pedestals subtraction is also performed.

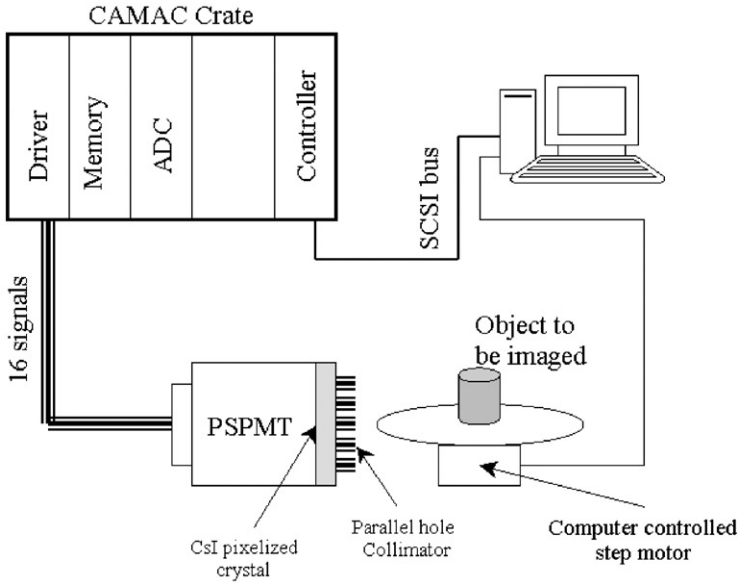

Fig. 1. Experimental setup.

3. Image reconstruction

The projection data at each angle are a 41×41 matrix, which is determined by the number of crystal pixels. The size of each pixel is 1.13 mm × 1.13 mm in space. The crystal is circular thus values of the data matrix near the corners are zero.

By rotating the object around its axis from 0° to 350° with a 10° step, 36 projections are obtained. Using a FBP [9,10] and MLA [11,12] algorithm slices of the object are reconstructed. Each line of the matrix represents projection data from one horizontal line and thus 41 slices can be reconstructed. However, due to insufficient number of crystal pixels at the top and the bottom, the first and last three slices suffer from poor resolution and they are excluded from 3D reconstruction.

4. System evaluation

The system evaluation has been carried out by the use of phantoms and small animals.

4.1. Phantoms

In order to evaluate spatial resolution of the system in planar imaging, capillaries with inner diameter of 1.1 mm and outer diameter of 1.5 mm, filled with ^{99m}Tc water solution, were used. In Fig. 2(a) four capillaries filled with solution with concentration ratios $1:\frac{1}{2}:\frac{1}{4}:\frac{1}{8}$ were placed at 2 mm distances in order to evaluate resolution and the ability of the system to detect activity variations. In Fig. 2(b) 11 capillaries filled with the same solution were placed at 2 mm distances in order to assess resolution and linearity in the whole field of view. It is clear that 2 mm spatial resolution and good linearity and sensitivity to activity changes are maintained in planar imaging in the entire field of view.

The system's evaluation for 3D imaging was performed by the use of capillary phantoms placed in 2–5 mm distances. FBP and MLA reconstruction algorithms were used and compared. For the 1.13 mm detector spacing the Nyquist criterion requires 70 angles over 180° for adequate angular sampling with a radius of rotation (ROR) of 2.5 cm. In this case the acquisition time would be

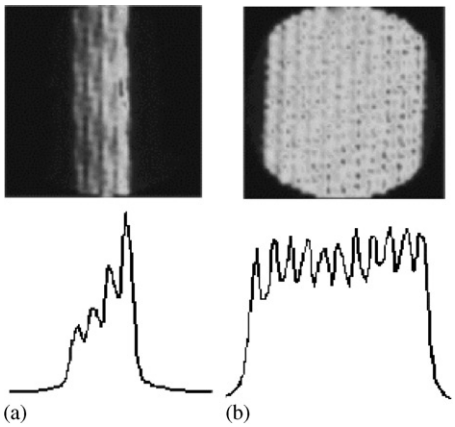

Fig. 2. Planar images and line profiles of 1.2 mm ID capillaries at 2 mm distances. (a) Four capillaries filled with ^{99m}Tc water solution with relative activity ratios (right to left) $1:\frac{1}{2}:\frac{1}{4}:\frac{1}{8}$. (b) Eleven capillaries filled with ^{99m}Tc water solution of the same activity.

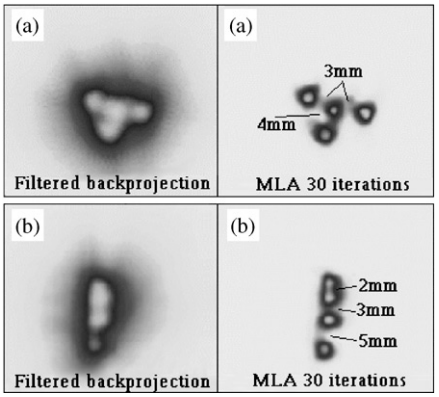

Fig. 3. Tomographic images of 1.2 mm ID capillaries at 2–5 intercapillary distances. Comparison of FBP (left) and MLA (right) after 30 iterations. (a) four capillaries at 3 and 4 mm distances (b), four capillaries at 2, 3 and 5 mm distances

unacceptable for a clinical test. In addition the star artifacts that arise from the use of FBP decrease resolution, whereas the MLA algorithm allows tomographic reconstruction from an incomplete data set with high signal-to-noise ratio. In Fig. 3, slices of capillary phantoms reconstructed with FBP (left) and MLA (right) are shown. It is clear that 2 mm resolution can be achieved in 3D imaging when the MLA is used. Thus the MLA was used in all of the following experiments.

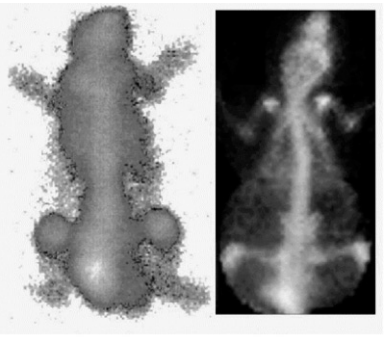

Fig. 4. Mouse injected with ^{99m}Tc-MDP. Comparative image of a hospital pinhole collimator camera (left) and the PSPMT camera (right).

4.2. Small animals

Comparative small animal imaging with a hospital gamma camera equipped with a pinhole collimator verified the superior resolution and sensitivity of the system for small organs imaging. In Fig. 4, the image of a mouse injected with ^{99m}Tc-methylene diphosphonate (MDP) is presented. The image obtained with the PSPMT system is clearer and provides many more details of the skeleton structure than the one obtained with the pinhole collimator camera.

5. Results

5.1. Image quality versus time

The detection of a spot in a "hot" background requires a satisfactory number of counts. It is thus important to investigate the image quality as a function of time. A square phantom (Fig. 5(a)) consisting of three levels, two circular and one square with 5, 10 and 15 mm depths, was filled with a ^{99m}Tc water solution and data were acquired for 2, 4, 10 and 20 min. The results, expressed in total counts and counts per mm^2 of the detector, are given in Table 1. The images acquired are shown in Fig. 5(b). In Fig. 5(c), line profiles at the center of the images are shown.

As it can be seen out from the images and the diagrams the quality of the image seems not to

Table 1
Total counts and counts/mm^2 as a function of acquisition time

Time (min)	2	4	10	20
Total counts	35,000	80,000	216,000	416,000
Counts/mm^2	21	48	129	250

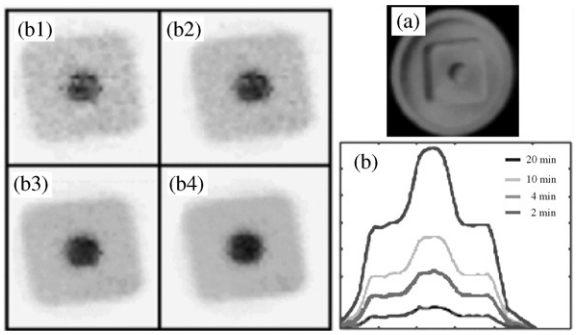

Fig. 5. Images ((b1) at 2 min, (b2) at 4 min, (b3) at 10 min and (b4) at 20 min) of the phantom (a) and line profiles at the center of the phantom (c).

improve significantly after the first 10 min of acquisition. We conclude that about 100 c/mm^2 are sufficient.

5.2. Paraffin phantom

In order to simulate breast tissue a paraffin cylindrical phantom was used. Thus the system resolution in 3D was estimated as a function of paraffin absorption and the distance from the detector. Four capillaries, 1.1 mm inner diameter (ID) and 1.5 outer diameter, were filled with ^{99m}Tc water solutions of relative activity ratios $1 : \frac{1}{2} : \frac{1}{4} : \frac{1}{8}$ and they were placed inside the paraffin cylinder in 2–5 mm distances. Two capillaries were 7 cm long whereas the other two were 5 cm long. The paraffin phantom was 6 cm in diameter and it was placed so that its axis was at 4 cm distance from the detector's surface. The capillaries-to-detector distance was 3.5–4 cm.The schematic diagram of the phantom is shown in Fig. 6.

In Fig. 7, slices 10, 15, 20, 25, 30, 35 are presented. It can be seen that in slices 10 and 15 only the two longer capillaries are visible as

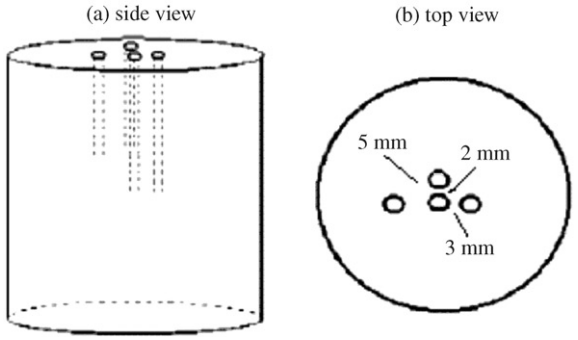

Fig. 6. Schematic diagram of the paraffin phantom. (a) Side, (b) top view.

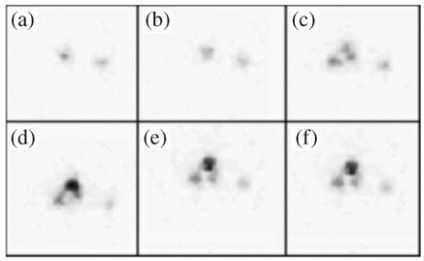

Fig. 7. Tomographic slices of the paraffin phantom. (a) slice 10, (b) slice 15, (c) slice 20, (d) slice 25, (e) slice 30 and (f) slice 35.

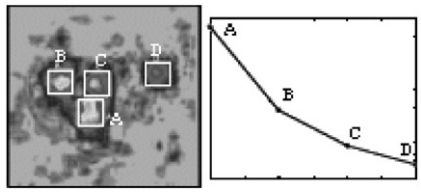

Fig. 8. Paraffin phantom. (a) ROIs in a typical slice. (b) The total number of counts for each ROI (relative scale).

expected. In slice 20 the third capillary is visible and the fourth one (with higher activity) starts to appear. In slices 25, 30 and 35 all four capillaries are imaged and their differences in activity are clearly depicted.

If we take regions of interest (ROIs) around the capillaries on a typical slice it is seen that the total number of counts is proportional to the activity of every capillary. In Fig. 8, the ROIs and the total number of counts are shown.

5.3. Cylindrical phantom-planar images

A cylindrical phantom was used for the evaluation of the sensitivity of the system. The cylinder was 10 cm in diameter and was filled with 200 ml of a 30 μCi ^{99m}Tc water solution in order to simulate the tissue background. Inside the cylinder a 1 cm ID tube containing a small quantity of a higher activity ^{99m}Tc solution was placed in order to simulate the tumor to be detected. A smaller tube, filled with background solution, was placed inside the 1 cm tube and above the higher activity solution in order to fill the "cold" area over the "tumor". The experimental setup is shown in Fig. 9.

Several tests with different combinations of "hot" spot volumes and activities were performed in order to measure the sensitivity. The "hot" spot to background activity ratio varied from 6:1 to 2:1 and the "hot" spot to background volume ratio varied from $\frac{1}{1000}$ to $\frac{4}{1000}$.

Data were acquired from 2 to 10 min in order to estimate the appropriate acquisition intervals. For a 0.2 ml "hot" spot with spot to background activity ratio 6:1 the images acquired for 2, 5 and 10 min and the line profiles at the center of the "hot" spot are shown in Fig. 10. Image counts are given in Table 2.

As it was pointed out in the previous phantom tests, the acquisition time must be about 10 min, so that an average of more than 100 counts/mm^2 are collected. In all the experiments the acquisition time was 10 min.

For a 0.2 ml "hot" spot volume the spot was clearly visible only when its activity was 6 times higher than that of the background. In Fig. 11, two images of 0.2 ml spots with tumor to background activity ratios 6:1 and 4:1 are shown. As it can be seen from the images and the line profiles only the "hot" spots in the first case is clear.

In Fig. 12, five images of 0.8 ml spots with tumor to background activity ratios 6:1, 5:1, 4:1, 3:1 and 2:1 and their line profiles are shown. The 0.8 ml "hot "spot is clearly being seen in the first three cases and it is visible in the latter two.

In Table 3, the set of parameters producing detectable images are given. It is seen as the "hot" spot volume increases the spot becomes detectable in a smaller "hot" spot to background activity ratio. The corresponding images are shown in Fig. 13.

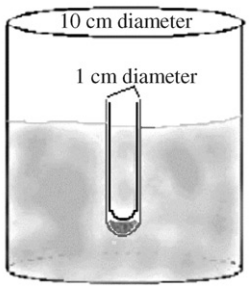

Fig. 9. Schematic diagram of the cylindrical ^{99m}Tc water solution phantom.

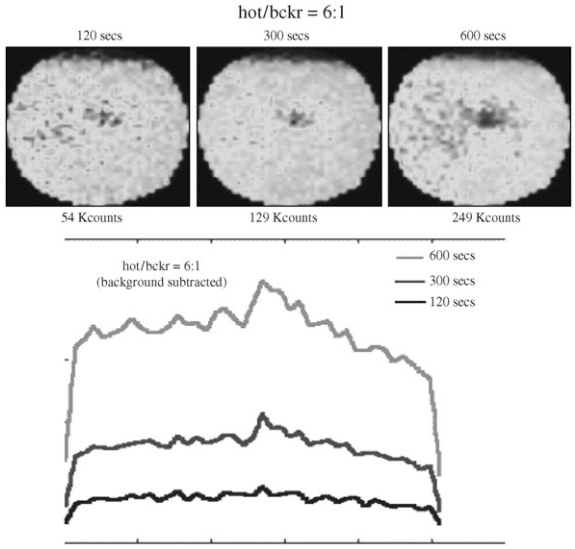

Fig. 10. Images and line profiles of a 0.2 ml "hot" spot with 6:1 spot to background ratio after 2,5 and 10 min.

Table 2
Total counts and counts per mm^2 vs. acquisition time in the cylindrical phantom

Image	a	b	c
Time (min)	2	5	10
Total counts	54,000	129,000	249,000
Counts/mm^2	32	77	149

5.4. Cylindrical phantom-SPECT images

In order to investigate the possibility that SPECT imaging could increase the "tumor" to background ratio a low statistics case was selected. As the phantom tests have shown if a "hot" source can be detected in 2D imaging it is detectable in 3D imaging as well. The aim of this experiment was to use a relatively short acquisition time, take few counts (20,000 or 12 counts/mm^2, which is almost 10 times less than the appropriate number) per projection and see if the spot could be detected in tomographic images.

The source volume was 0.4 ml while the background volume was 200 ml and the activity ratio was 4:1. Approximately 20,000 counts were collected in each projection. In Fig. 14 an image of that source with 20,000 counts is compared to a corresponding image of 100,000 counts. It is clear that planar images with 20,000 counts cannot provide clear depiction of the source.

The phantom was then rotated around its axis with a step motor and 36 projections were obtained. Nine slices have been obtained around

Table 3
Set of parameters producing detectable images

Phantom number	1	2	3	4
Tumor volume (ml)	0.2	0.4	0.6	0.8
Tumor to background volume ratio	0.001	0.002	0.003	0.004
Tumor to background activity ratio	6:1	5:1	4:1	3:1

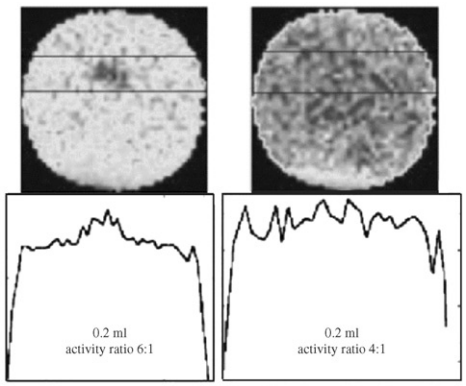

Fig. 11. Four images of 0.2 ml spots with tumor to background activity ratios 6:1, 4:1, 3:1 and 2:1 and their line profiles. Data were collected for 10 min.

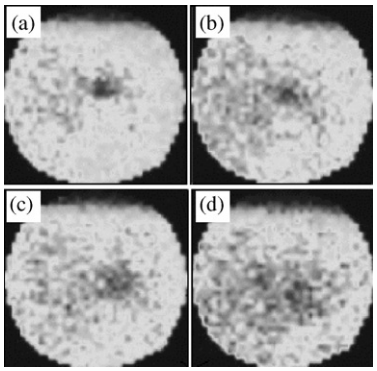

Fig. 13. Images of 0.2 (a), 0.4 (b), 0.6 (c) and 0.8 ml (d) spots with tumor to background activity ratios 6:1, 5:1, 4:1 and 3:1, respectively.

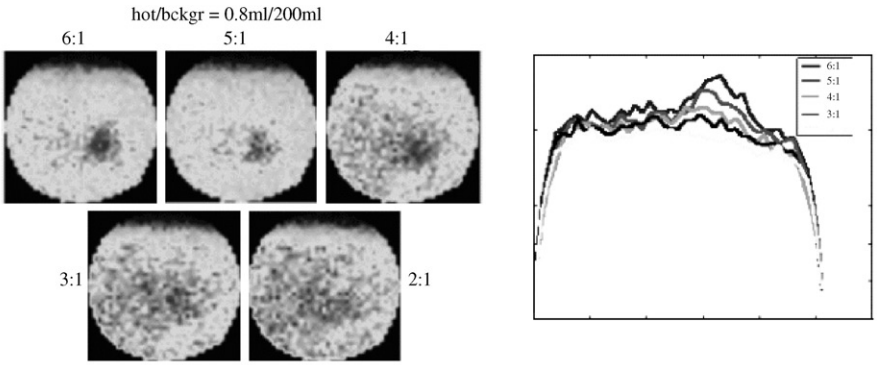

Fig. 12. Five images of 0.8 ml spots with tumor to background activity ratios 6:1, 5:1, 4:1, 3:1 and 2:1 and their line profiles.

the "hot" spot area whose height is 4–5 mm.The spot is clearly depicted in slices 3–6 and less in slices 2, 7 and 8. The slice images and a typical line profile are shown in Fig. 15. It is clear that the spot can be depicted. Although some noise artifacts, which are amplified by the MLA algorithm due to low statistics, are present it can be said that SPECT imaging offers higher sensitivity than planar imaging especially in low statistic cases.

6. Conclusions

The potential of a small field of view gamma camera based on a Position Sensitive Photomultiplier Tube and a crystal, made of CsI(Tl) to image breast phantoms has been examined. The system has been tested with phantoms and offers a spatial resolution of 2–3 mm both in planar and tomographic mode. The use of a paraffin phantom, which simulates tissue absorption properties, has shown that with the use of Maximum Likelihood Algorithm 2–3 mm resolution is achieved in 3D. Moreover, the system is very sensitive in detecting activity variations. Experiments with a cylindrical phantom filled with ^{99m}Tc water solution that simulates tissue background activity have shown that "hot" spots with small volume (0.2 ml to 0.4 ml) and low spot-to-background activity ratio (6:1 to 5:1) can be detected.

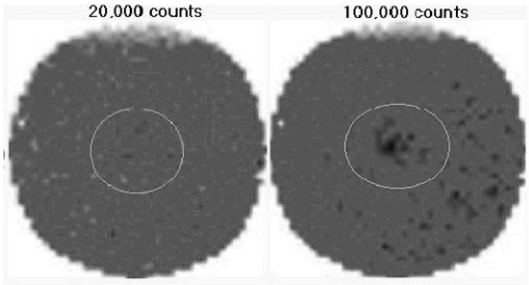

Fig. 14. Comparison of images of a 0.4 ml source with source to background ratio 4:1 for 20,000 (left) and 100,000 (right) acquired counts.

References

[1] H.O. Anger, IEEE Trans. Nucl. Sci. NS-13 (1996) 380.
[2] R. Pani, R. Pellegrini, F. Scopinaro, et al., Nucl. Instr. and Meth. A 392 (1987) 295.
[3] R. Pani, R. Pellegrini, A. Soluri, G. De Vincentis, et al., IEEE Trans. Nucl. Sci. NS-43 (6) (1996) 3264.
[4] A. Weisenberger, Gamma ray imaging detector for small animal research, Ph.D. Dissertation, The College of William and Mary in Virginia, August 1998.
[5] S. Majewski, F. Farzanpay, A. Goode, Nucl. Instr. and Meth. A 409 (1998) 520.
[6] G. Kontaxakis, L. Strauss, Maximum Likelihood Algorithms for Image Reconstruction in Positron Emission Tomography, Mediterra, Athens, 1998.
[7] S. Archimandritis, N. Giokaris, A. Karabarbounis, G. Loudos, D. Maintas, S. Majewski, K. Nikita, R. Pani, C. Papanicolas, F. Scopinaro, C. Stefanis, E. Styliaris, N. Uzunoglou, A. Varvarigou, A. Weisenberger, R. Wojcik, A high resolution gamma-ray camera for small animals imaging, Frontier detectors for frontier physics, Eight Pisa Meeting on Advanced Detectors, La Biodola, Isola d'Elba, Italy, May 21–27, 2000.
[8] G.K. Loudos, K.S. Nikita, N.A. Mouravliansky, N.K. Uzunoglu, G. K. Matsopoulos N.D. Giokaris, A. Karabarbounis, C.N. Papanicolas, E. Styliaris, S.C.

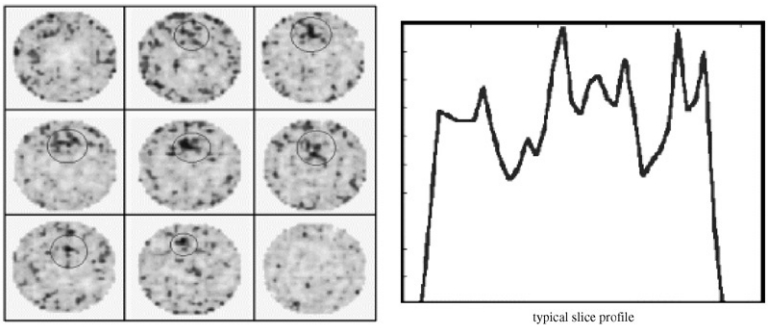

Fig. 15. Nine successive slices of a 0.4 ml source with source to background ratio 4:1 (left) and a typical line profile (right).

Archimandritis, A.D. Varvarigou, D. Maintas, K. Stefanis, An assessment of position sensitive photomultiplier tubes for high resolution 3D imaging, IEEE, Nuclear Science Symposium and Medical Imaging, Lyon, 15–20 October 2000.

[9] C. Kak, Slaney, Principles of Computerized Tomographic Imaging, IEEE Press, New York, 1987.

[10] G.T. Herman, Image Reconstruction from Projections. The Fundamentals of Computerized Tomography, Academic Press, New York, 1980.

[11] L.A. Shepp, Y. Vardi, IEEE Trans. Med. Imaging 1 (2) (1982) 113.

[12] K. Lange, M. Bahn, R. Little, IEEE Trans. Med. Imaging 6 (2) (1987) 106.